Experimental study of crease formation in an axially compressed sheet

Sahraoui Chaïeb and Francisco Melo
Departamento de Física de la Universidad de Santiago, Avenida Ecuador 3493, Casilla 307, Correo 2, Santiago, Chile
(Received 26 March 1997)

In our study of crease formation in a cylindrical panel subject to axial compression, we found that the maximum vertical deflection ζ increases in the orthoradial direction l and saturates when the panel is larger than half a cylinder. The length of the crease X decreases by increasing the panel opening angle, and saturates to a constant value when the opening angle is close to 2π. The stress corresponding to initial crease formation goes as $1/R$, where R is the radius of curvature of the panel. Profilometric measurements reveal the presence of a region around the singularity where the stress is focused and where the deformation is plastic. [S1063-651X(97)03009-2]

PACS number(s): 46.30.Lx, 62.20.Fe, 68.55.Jk

I. INTRODUCTION

Thin plates or membranes in a crumpled state occur in many systems at various aspects and length scales, from membranes of polymerized phospholipids to crashing of cars and cans [1–4]. A crumpled sheet is characterized by a distribution over its surface of sharp ridges and permanent creases. Each crease terminates in pointlike defects or *singularities*, which are points where the yield limit of the material has been exceeded [5]. Unlike phospholipidic membranes, the crumpling of a sheet of macroscopic elastic material (paper, aluminum, copper, polypropylene, etc.) requires compression, such as we apply in making a paper ball. In this case, scars left after the crumpling process are due to the focusing of the stress at singularities.

From a theoretical point of view, the relation between the geometric aspects of the formation of an isolated singularity on a surface and the singularities mechanical origin is relatively well understood. One of the key points is that particular solutions of the Föppl–von Kármán (FvK) equations describing large deformations of thin plates are developable cones [5]. It is important to notice that developable surfaces and particularly developable cones are obtained from, or applied to, a plane without changing distances. They have zero Gaussian curvature, and nonzero mean curvature [6]. A d cone has two regions of opposite curvature, one convex and the other concave. The concave region is separated from the convex region by two ridges (Fig. 1). Another characteristic of d cones is that any circle of radius r whose center is at the singularity has its perimeter $2\pi r$ after the d cone is formed as well; i.e., the mapping between a plane and a d cone is isometric [7].

Even though the FvK equations do not explicitly include an initial curvature, singular solutions are possible. In practice, in order to generate singularities in a sheet, it is necessary to bend it, pushing the bent sheet in the axial direction causes singularities to nucleate. For instance, when the two edges of a flat sheet of paper are pushed together, one observes only a wavy pattern: no creases, sharp ridges, or singularities appear. The equations used when an initial curvature is introduced are commonly called the Donnell equations, and are a slight modification of the FvK equations [8–10]. To our knowledge, the Donnell equations have not been studied systematically.

Further studies based on FvK equations obtained a useful relation between the deformation energy and the size of a ridge in a bent sheet [1,11,12] by using scaling arguments and boundary layer analysis. Additionally, an efficient numerical method to solve the FvK equations in the case of a crumpled sheet was proposed [13]. These works were successful in describing the main features of a simple crumpled surface, but none has considered realistic boundary conditions. Numerical methods seem more suitable to investigate boundary conditions effects [1,13].

Experimentally, a well-controlled nucleation of singularity is not an easy task. However, apart from a crumpled sheet of paper, singularities can be seen in a postbuckled cylinder. Since the pioneering work of von Kármán and co-workers [10,14], several studies were devoted to initial stage cylinder buckling for industrial and aeronautical purposes [10,14–16]. At the first stage of cylinder buckling a pattern of squares appears. Singularities were not investigated, as they appear only when the cylinder is postbuckled. Although von Kármán predicted that for short cylinders in the postbuckling regime sharp ridges and narrow diamonds appear, none of these experiments reported studies either on singularities or on short cylinders (the singularity appears at the meeting point of four squares). However, it was stated that narrow diamonds could have been seen in the case of short cylinders

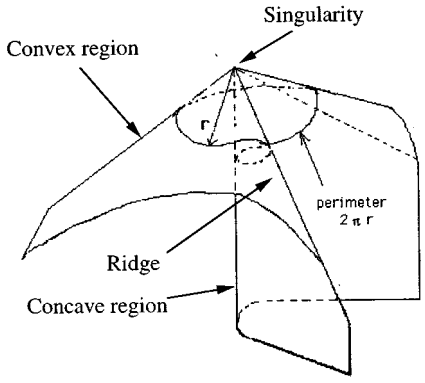

FIG. 1. A d cone obtained by bending and compressing a planar sheet.

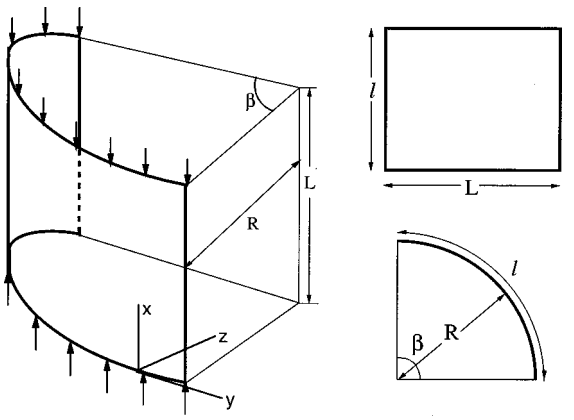

FIG. 2. The geometry used in our experiment. Right top is a side view, and the bottom is an end view.

[16]. Further studies focused on the effect of initial irregularities on the critical load and on the postbuckling equilibrium load. It was shown that although initial imperfections were not eliminated, the results were reproducible under the same experimental conditions [15].

In this paper we study the nucleation of singularities in a thin cylindrical panel submitted to axial compression. We show that, in this case, a crease can be seen as two opposite d cones which tips are separated by a distance equal to the crease length. In the following, the crease length X is the distance separating the two singularities, and the ridge is the line shown in Fig. 7. We investigate mechanical and geometric properties of creases, namely, critical load, radius of curvature, and characteristic sizes as a function of geometric parameters.

This paper begins with a description of the experimental setup and sample preparations. In Secs. III and IV, we describe the patterns observed in both narrow and wide panels. Section IV includes measurements of the global properties of the patterns (vertical deflection and crease length). In Sec. V, we present results concerning the critical load and its dependence on the radius of the panel. Section VI is devoted to local properties of a single crease. Finally, a conclusion is presented.

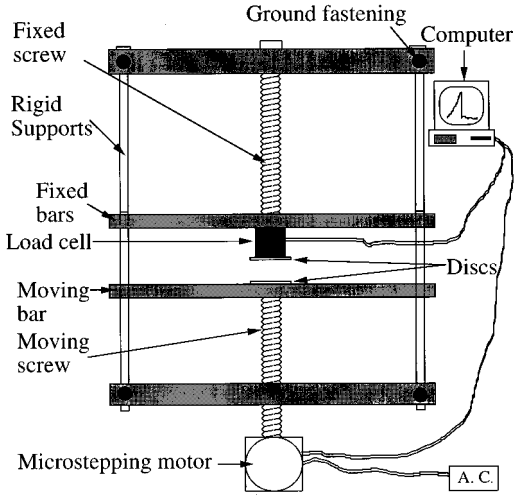

FIG. 3. The compression machine.

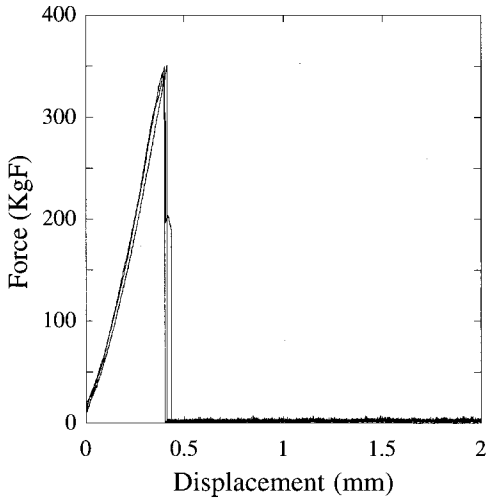

FIG. 4. Three different runs, under the same conditions, showing the load vs the displacement δ for a panel under compression. The parameters are $L=90$ mm, $l=60$ mm, and $R=32.7$ mm.

II. EXPERIMENTAL CONSIDERATION

We submit a panel of thickness h, width l in the circumferential direction, length L, opening angle β, and radius R to axial compression (Fig. 2). We chose this geometry because it is the simplest curved surface one can crumple. It is possible to consider a hyperbolic or parabolic shape, but such surfaces lie in the same class as the cylinder, and we expect no qualitative difference with respect to the nucleation of singularities.

Our cylindrical panels are 0.1-mm-thick sheets of DHP copper. The thickness of the panels is constant within 1%. Such panels are obtained by cold rolling a thicker plate. This process produces what is called residual forces within the bulk of the plate, and creates an anisotropy with respect to the two in-plane directions, parallel and perpendicular to the rolling direction. In order to eliminate the flattening induced strain of the grains, we anneal the sheet [17,18]. The residual stress is checked by measuring the deformation of the unit cell of the copper crystal with respect to a cubic one using x-ray diffraction.

Cylindrical shells are compressed by a machine which consists of two parallel arms. One arm is fixed, while the other is moved smoothly at a constant compression rate monitored by a microstepping motor (Parker, Compumotor). The moving arm is pushed toward a fixed arm by a screw ball of diameter 30 mm. A vertical disc with a series of 0.2-mm-wide and 2-mm-deep concentric grooves is mounted on each arm. The radius of the grooves varies from 13.9 to 58.45 mm. One disc is connected to a load cell (Revere R_T Transducers Inc. Model 363/9363 Cerritos, CA) which measures the force on the sample. The load cell is connected to a computer which stores and analyzes the data (Fig. 3). We have checked the rigidity of our load cell, and found that any possible shortening, due to deformations, is less than 5×10^{-5} mm/kgf over a panel's deformation of about 4 mm and a force range of 1000 kgf. The load cell is capable of resolving 0.5 kgf over a range of 1000 kgf.

To check the parallelism of the two disks we simultaneously compress two panels of the same size and the same

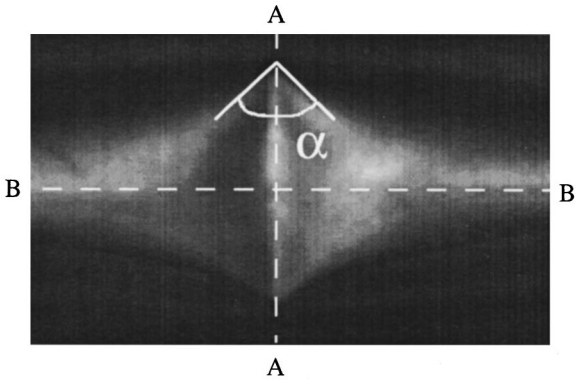

FIG. 5. A crease which appears in the middle of a small opening angle panel. The cuts *AA* and *BB* are the line followed by the profilometer and called longitudinal and transversal directions in Fig. 12.

radius by placing the panels opposite each other between the two discs. When the two discs are parallel, the buckling force must be twice the buckling force of a single panel. The compression rate is kept low (0.01 mm/s), which reduces the effects of initial off-plane imperfections and irregularities of the clamped edges due to motion and initial misalignment of the panel within the grooves. Although it was shown theoretically [19] that imperfections, curved edges near the grooves, have no serious effects on the magnitude of the critical force, since they are damped out exponentially in the compression direction [20], we nevertheless attempt to avoid them. Initial imperfections can sometimes lower the critical load [10]. It was also shown in experiments on closed cylinders that the postbuckling load is insensitive to initial irregularities [15]. In contrast, we observed that the pattern structure is strongly affected by initial imperfections, such as small deflections of the clamped edges on which the panel is supported or the nonparallelism of the panel. For instance, an initial angle of the order of a hundredth of a radian between the supporting edges can affect the results. The critical force corresponds to the occurrence of a crease, but it is difficult to characterize because the crease nucleation resembles a sub-

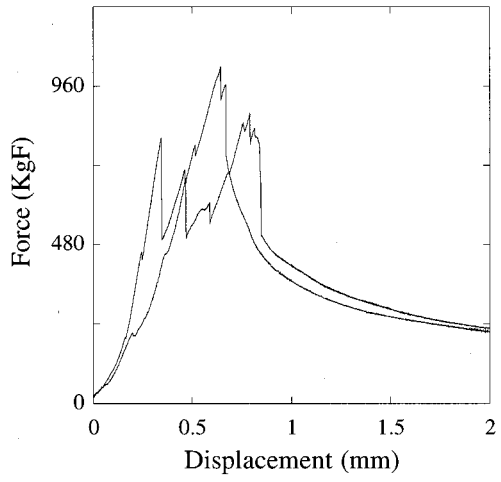

FIG. 6. Force vs the displacement for $\beta=4.3$. Note the secondary peaks before the maximum load; each one corresponds to the nucleation of a crease.

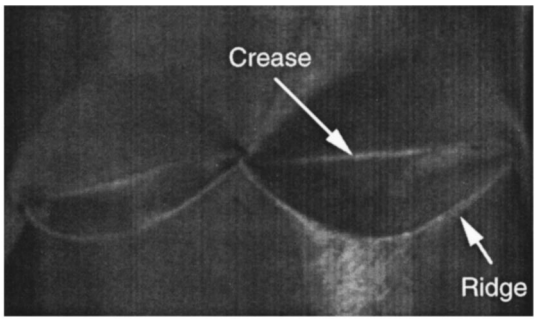

FIG. 7. The structure observed when compressing a large panel. With further compression, another series of creases appears and the chain of creases develops in the circumferential direction. The opening angle in this case is 4.33 rad.

critical transition, and the creases that fill the panel do not all appear at the same time. We then measure the maximum force necessary to buckle the panel. The jump in equilibrium position as the crease appears involves a release of elastic energy, and thus explains the rapidity of the buckling process justifying the subcritical character of the transition.

In our experiments, contrary to the case for full cylinders, one has an additional parameter, the opening angle β in Fig. 2, which is variable. The dependence of the crease properties on l, R, and β is discussed in the following sections.

III. SMALL OPENING ANGLE

The results discussed in this section are obtained for β less than 2 rad. The critical force necessary to create a crease for three different runs under the same conditions corresponds to the peaks in Fig. 4. During compression, the force increases nearly linearly except at the beginning of the loading when the panel slides into the grooves. Even though such rearrangements occur, the critical force is reproducible to within 5%.

For the runs shown in Fig. 4 and for all lengths L, the critical load is equal to the maximum load necessary to collapse the panel. At the critical force, the stored elastic energy is released abruptly by forming a crease at the middle of the panel. From Fig. 5, one can see that a crease is composed of two opposite d cones with common concave parts. In the following, the line limiting the crease deflection and the rest

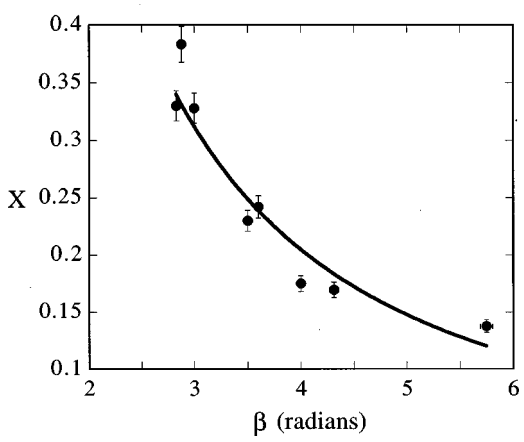

FIG. 8. Normalized crease length vs the opening angle β.

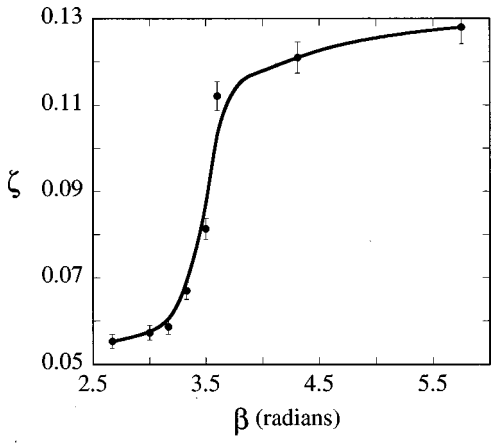

FIG. 9. Normalized vertical deflection vs the opening angle β in radians.

of the panel will be called the *ridge*, and the line joining the singularities will be called the *crease length*. The distance between the d-cone vertices is the crease length X.

We measured the diamond-shaped pattern opening angle α (α is defined in Fig. 5), and found it to be of the order of 88°, close to the value of 90° observed for a closed cylinder [9]. For panel lengths larger than $5R$, the strip buckles like a rectangular strip after the occurrence of a crease [21]. However, for narrow panels with an intermediate opening angle, while keeping the panel under compression the tip of the crease propagates toward the free borders and leaves behind a wake of high curvature. This phenomena, which shows the presence of a dynamic of the tip, will be the object of future work.

We remark that for closed cylinders the wavelength of the pattern in the direction parallel to the compression is given by the radius of the cylinder times the thickness [19]. However, in our case the size of the crease is also selected by the opening angle. This point will be described later in the text.

IV. LARGE OPENING ANGLE

In this section, the results obtained correspond to an opening angle β larger than 2 rad. Figure 6 shows the loading force versus displacement; several peaks occur before the maximal load after which the force decreases. These secondary peaks correspond to the nucleation of creases. The last and maximum peak corresponds to the buckling of the whole panel, after which no more creases appear. The load, after the maximum for small β (Fig. 4) decreases more rapidly than the load for large β (Fig. 6): In the first case, the panel is folded after the first crease appears.

The structure observed after all the creases have appeared resembles a string of diamonds (Fig. 7) similar to those observed in experiments on thin compressed circular cylinders, although they have observed only squared creases [15,8]. The angle α is smaller than the angle in the case for closed cylinders. In this case the creases are more flattened. The vertical deflection is more pronounced, and the diamonds flanks are sharper. We measured the angle α of these diamond-shaped patterns and found it to be between 75° and 80°, and independent of the opening angle, but smaller than the value of 90° predicted theoretically [9].

If one leaves a long buckled panel under compression, another series of diamonds appears, filling the panel in the x direction. In this work we considered only the first series, as the second one appears after the first diamonds have been totally folded, which affects the length L of the panel. As the width increases, the number of creases and the wavelength (size of each crease) selected also increase. The crease length X decreases, as is shown in Fig. 8, where we plot the crease length normalized by the radius.

One can observe that the crease length X decreases very quickly when β goes to 2π. For $\beta \sim 2\pi$ the crease length saturates to a value X_0 which, we believe, corresponds to the crease length for closed cylinders. We also measured the maximum vertical deflection ζ as a function of the opening angle β. The vertical deflection increases when the angle β increases, and tends to saturate when the panel is larger than a half cylinder, i.e., $\beta \sim \pi$. Figure 9 shows the variations of the maximum vertical deflection versus the opening angle. We believe that, when the opening angle approaches 2π, the vertical deflection goes to a value which corresponds to vertical deflections in the case of a buckled closed cylinder. As both crease length and maximum deflection saturate when the opening angle approaches 2π, we measured the length crease for $\beta = 6$ rad as a function of the panel radius R for a length $L = 40$ mm. Figure 10 shows the variations of the crease length with the radius of the panel. From the linear fit to the curve, $X \sim 0.7R$. In our experiment, the singularities and creases nucleate in a subcritical way, releasing the elastic energy stored in the panel during the compression. The creases appear suddenly by causing an inward deflection in the panel. von Kármán and Tsien predicted that in the case of thin closed cylinders the wavelength of the pattern is given by the ratio of the radius to the thickness. The transition from squares to ellipses is controlled by the ratio of the wave amplitude of the cylindrical shell buckled shape and the thickness, but this model failed to give these sharp diamonds at large deflections [10]. We also notice, for a fixed large opening angle, that the creases are self-similar. In fact, by increasing the radius of the panel we increase in the same way the distance which separates the d cones' tips that fit in the panel. The lateral dimension of the crease, in the direction of the load (the x direction), also increases with the radius. In the next paragraph we will show why the crease

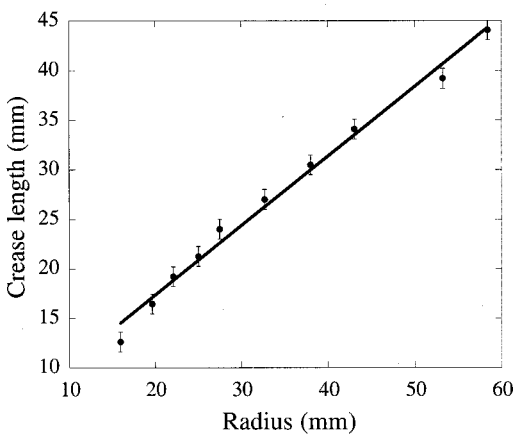

FIG. 10. Crease length X as a function of the panel radius for $\beta = 6$ rad, $L = 40$ mm.

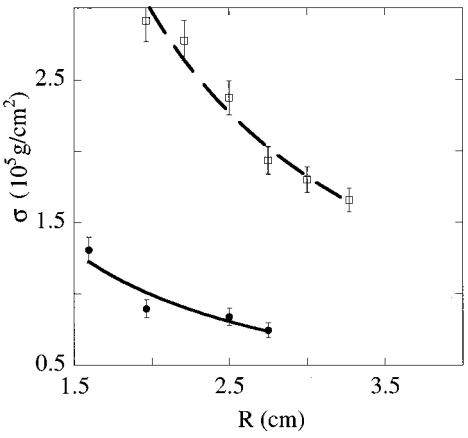

FIG. 11. The maximum stress vs the radius R of the panel for two different opening angles β.

depends in such a way versus the radius.

To explain the origin of the creases self-similarity and the reason for the dependence of X on R for a large opening angle, we assume that the energy of a buckled panel can be separated into two contributions, namely, the crease curvature energy far from the singularities, and the singularity energy. Subsequently, we will show how the competition between these energies determines the selection of the creases length. The curvature energy of the crease far from the singularities, without the term containing the Gaussian curvature is, $E_b = D\int ds(\nabla^2\zeta)^2$, where D is the rigidity and is equal to $Eh^3/24(1-\sigma^2)$ [22]. Following Refs. [1,12,22], we can evaluate this energy far from the two singularities, i.e., in a strip of length X, depth ζ, and width d. The width of the strip is the distance separating the two flanks of the crease at midcrease. If we suppose that the off-plane variations of the sheet are dominated by contributions in the direction perpendicular to the crease length (in other words, $\nabla^2\zeta \sim \partial^2\zeta/\partial x^2$), we find that $E_b \sim DX^5/d^3R^2$, where R is the radius of the panel. As the structure we observe is composed of lozenges, $d \sim AX$, where A is a constant close to 1. We then find $E_b \sim DX^2/AR^2$. Per unit length, the bending energy can then be written as DX/AR^2. As a consequence of the creases' self-similarity, we assume that the energy of the singularity ϵ_p is constant and does not depend on the typical sizes in the problem, namely, the panel radius and the crease length. As the stress is focused at the singularities, this energy should contain all the contributions including the stretching energy. The singularity energy per unit length is then $2\epsilon_p/X$. The factor 2 corresponds to the fact that each crease is bounded by two singularities. The total energy per unit length is then $\mathcal{F} = DX/AR^2 + 2\epsilon_p/X$. Minimizing $\mathcal{F}$ with respect to X gives $X^2 \sim (2A\epsilon_p/D)R^2$. In the argument above we assumed that the contribution to the crease bending energy was essentially due to the crease curvature far away from the singularities after the creases had nucleated; we did not take into account membrane bending in the longitudinal direction (the line joining the singularities is itself slightly bent). Also, as the scaling is performed far from the cone tip, we did not take into account logarithmic contributions to the bending energy [5,24–26]. As the creases are self-similar (for an opening angle β at which the crease length and the vertical deflection saturate), the singularity energy was assumed constant (or a slowly varying function of the opening angle β), and independent of the length scales in the problem. As a result of the competition between a bending energy which favors large creases and a singularity energy which favors small creases, we found that $X \sim R$, in agreement with the experimental results of Fig. 10 and with the fact that the singularity energy is constant and independent of the crease length and of the panel radius. From the best fit to the curve in Fig. 10, we find that $\epsilon_p \sim 0.25D$.

The d-cone opening angle is related to our experimental angle β. In fact, for a given R, smaller is β, is the d-cone angle is higher. If we fix the opening angle (at which the crease saturates), and vary the radius as in Fig. 10, fit the same crease number in the panel, and the same d-cone number, the distance between the d-cone vertices will then vary. On the other hand, if we fix the radius and vary the opening angle, the number of the creases vary, and so do their lengths. The creases are no longer self-similar. The singularity curvature and energy are not constants.

We also studied panels for which the opening angle is large, but whose length is much larger than the radius [(3–4) R]. In this case the structure of the pattern depends drastically on the initial imperfections, and the stability of the shell is difficult to control. In addition, the size of the crease increases in the direction of the compression, and number in the circumferential direction decreases with the increasing length of the panel.

V. CRITICAL LOAD MEASUREMENT

For all cases, i.e., for $\beta < \pi$ and $\beta > \pi$, the maximum stress σ, measured as mentioned above, and defined as the force per unit area necessary to buckle the panel (the area is the quantity $h \times l$, where h and l are the thickness and the width of the panel, respectively) varies with the radius as $1/R$, in agreement with the theoretical results of von Kármán and Tsien [10], Koiter [23], and Timoshenko [19], for a cylinder or a cylindrical panel with periodic boundary conditions.

Figure 11 shows the maximum stress for two opening angles (smaller and larger than a half-cylinder). We do not emphasize this last result, as the critical force is difficult to measure because the occurrence of creases is sudden and subcritical. However, the fit to the curve gives a good order of magnitude of the Young modulus E of rolled copper. One can notice that for a larger width of the panel the experimental points collapse on a better fit. This is due to the fact that the free boundaries (that are the unclamped edges) have a stronger effect in the case of a panel with a small opening angle ($\beta < \pi$), for which the panel curvature is not necessarily kept constant during the compression. We also studied the variations of the stress as a function of the longitudinal direction, i.e., as a function of the length L of the cylindrical panel. We noticed no remarkable variation of the critical stress, except the one due to systematic experimental errors and noise.

VI. LOCAL PROPERTIES: PROFILOMETER MEASUREMENTS

In order to characterize the local geometry of the crease fully, we built a profilometer which consists of a moving

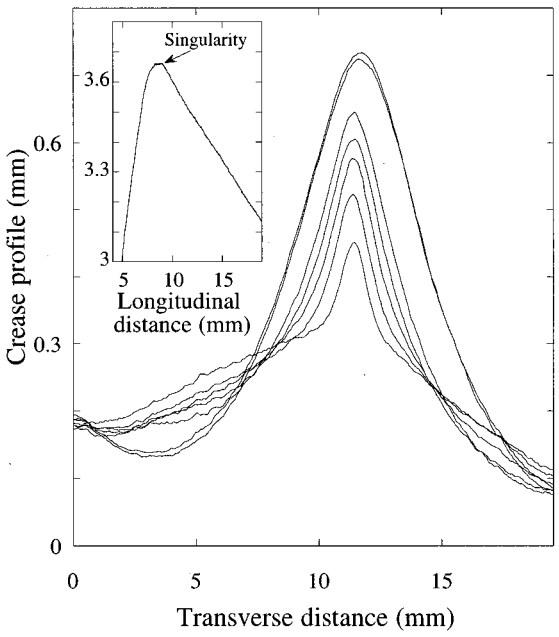

FIG. 12. The profiles of the crease along the transverse direction (cut along the direction *BB* in Fig. 5) for different positions along the crease. In the inset, we show the profile of the crease at the singularity, the scan is in the longitudinal direction along the crease (cut along the direction *AA* in Fig. 5) crossing the singularity.

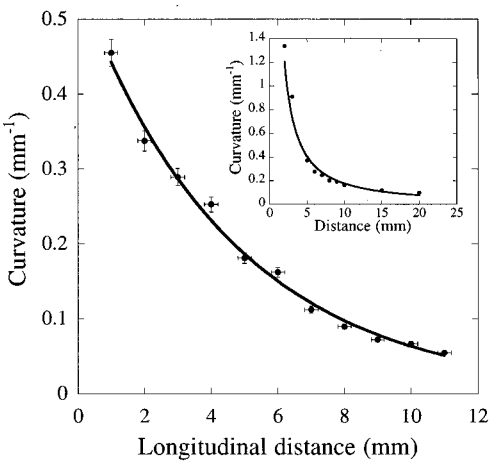

FIG. 13. The crease transverse curvature as a function of the longitudinal distance from the singularity. Inset: The curvature along the ridge vs the distance to the singularity of a *d* cone similar to the *d* cone of Fig. 1 and made of copper.

table and a tip connected to a transducer controlling the displacement of the tip. The moving table on which the sample is pasted has a constant velocity of 0.2 mm/s. This profilometer is able to resolve less than 0.01 mm in the vertical and horizontal directions. The whole is connected to a computer where the data are stored and treated.

In Fig. 12 we show different profiles of a 25-mm crease. These profiles are obtained by scanning the crease in the transverse direction of the crease (cut *BB* in Fig. 5). The different profiles correspond to different position from the singularity to the middle of the crease. It can be seen, approaching the singularity, that the profiles become sharper. In the inset of Fig. 12, we show the profile of the plate along the crease, called the longitudinal direction in the figure (also called cut *AA* in Fig. 5), and across the singularity. It is easy to notice a sharp cusp of the sheet at the singularity. In order to measure the curvature at the top of the profile in Fig. 12, we fit the profile tip to a parabola, and identify the parabola curvature with the crease curvature at the top of the crease. In Fig. 13 we plot the crease transverse curvature C as a function of the distance along the crease. In Fig. 13 the zero corresponds to the singularity. We observe that the curvature decreases when we move away from the singularity. The fit to the data is an exponential of the form $C_0 e^{-(r/d_c)}$, where C_0 is the curvature of the crease at the singularity, and is equal to 0.55 mm^{-1}, and d_c corresponds to a cutoff distance. This distance bounds the region where the curvature is concentrated, and where a permanent crescent shape is visible around the singularity.

In Ref. [5], the region near the *d*-cone tip where all the energies are of the same strength was called the *inner region*. In our experiment we find a natural *inner region* in which the deformation is mostly plastic and the extensional energy is of the same order of magnitude as the bending energy, which causes the permanent scar. The distance d_c is equal to 4.6 mm and corresponds to a radius of curvature $1/C$ of about 4.9 mm. We notice that the value of the curvature at the singularity is smaller than $1/h$, which means that the sheet is not totally folded, in which case its radius of curvature would be close to h. In order to support our arguments, let us find the curvature at which the plate suffers bending just beyond Hook's law (plastic deformation); we begin with a beam of rectangular cross section. We assume that the radius of curvature of the middle surface produced by bending is r. It is well known that the unit elongation of a fiber at distance y from the neutral surface is $\epsilon = y/r$. So the total deformation Δ (compression of the inner surface and tension of the outer region) is the sum of the maximum elongation and the maximum contraction; that is, $\Delta = h/r$, where h is the thickness of the plate. The Young modulus E is given by the fit to the curve in Fig. 11, with the formula giving the buckling stress versus the radius [10,8,19]. The slope in Fig. 4 also gives the same order of magnitude as the Young modulus (using Hook's law before buckling). From the expression $\sigma = \epsilon E$ and the maximum load in Fig. 4, we find a deformation of 2×10^{-2} which corresponds, in the case of a thickness of 0.1 mm, to a curvature and a radius of curvature of approximately 0.2 mm^{-1} and 5 mm, respectively.

The cutoff length is then of the same order as the critical radius of curvature necessary to produce a plastic deformation in the sample. In the following we check if the variations of the curvature with the distance from the singularity are independent on the geometry in which the *d* cone is obtained. We perform the same measurements as before for a *d* cone similar to the one shown in Fig. 1. Such a *d* cone is obtained by pushing a rounded tip on the center of a circular plate, along the plate principal axis, while keeping the border of the plate free to move in a circular frame of radius slightly smaller than the sample radius. The inset of Fig. 13 is the curvature of one of the ridges of such a *d* cone made in a plate of the same copper sheets (Fig. 1). From this figure one can notice that the curvature decreases exponentially when moving away from the singularity. From the best fit of the

curve we also obtain a characteristic distance on the order of 5 mm which is very close to the value obtained for cylindrical panels. Additional measurements, on the same d cones, have shown that the distance d_c does not depend on the d-cone opening angle when this latter is small. In this section we showed that the stress is focused in a region around the singularities whose radius is d_c. The stress is not distributed everywhere in the panel but is concentrated only at the singularities. If we evaluate the bending energy of a curved plate, having 5 mm as the radius of curvature, over a surface d_c^2, we find that it is of the same order of magnitude as ϵ_p introduced in Sec. IV.

VII. CONCLUSION

In this paper we investigated both the global and local properties of a crumpled cylindrical panel considered as a first approach to a real crumpled sheet. By compressing a cylindrical panel, we were able to nucleate creases, ending up with singularities. We found that cylindrical panels can be divided into two categories, depending on the opening angle β. The two categories are panels with small opening angles and panels with large opening angles. For the first category, only one crease appears, and it has almost the size of the width of the panel. This crease grows in size as the compression is kept, and the singularities are ejected out of the panel, leaving a wake of high curvature similar to the figures one can encounter in growth process. For a large opening angle, the structure is richer than the previous category. The creases appear as a set of d cones in opposition, geometrically situated in the direction perpendicular to the compression direction, and they depend on the topological and geometric characteristic of the panel under load. We also noticed that the panel opening angle is closely related to the opening angle of the d cones that form the crease. The number of creases that fit in the panel increases with β. Their size decreases with an increase of the panel opening angle β. The crease length and the maximum vertical deflection saturate as the opening angle approaches 2π. We measured the crease length X at $\beta \sim 2\pi$ and found that it goes like R. For $\beta \sim 2\pi$, the crease number is constant, and the crease lengths are like that of a closed cylinder. We found that this behavior is a consequence of the competition between the curvature energy of a large crease without a singularity and the singularity's contribution. This selection is due to the fact that, for a large panel, the appearance of several singularities compensates for the divergence of the bending energy corresponding to a large crease, which, when the singularity contribution is not taken into account, scales like X. As the creases are self-similar, we assumed in our scaling arguments that the energy of the singularity is constant at nucleation. This assumption is in agreement with our experimental results. We also neglected logarithmic contributions [25,24], as they are negligible with respect to the algebraic expression of the bending energy written above and also introduced in Refs. [1,12]. In fact, it is well known that for thin plates the bending energy is much smaller than the stretching energy [22]. Therefore, further compression leads to bending other regions and nucleating more creases rather than increasing the already existing deflections. From local measurements of the crease curvature, we could characterize a region where all the stress is focused and where the deformation is plastic. The curvature energy for a plastic deformation is of the same order of magnitude as the singularity energy. If we evaluate the curvature energy for a copper panel with a radius of curvature of 5 mm, we find that this is of the same order of magnitude as the singularity energy introduced previously. This energy is obtained by integrating the curvature squared over a circle of radius d_c, measured from profile measurements. Finally, we think that the singularity energy can be written properly in terms of the d-cone opening angle introduced in Refs. [5,24], as each singularity is the tip of a d cone. The pattern observed on a postbuckled panel is proof that the only developable surface mapped on a buckled cylinder is a d cone.

In the future we will explore an eventual dependence of the region of plastic deformation on the macroscopic size bounding the d cone. Further work exploring the dynamics of the singularities and their interactions is also underway.

ACKNOWLEDGMENTS

We are grateful to R. Labbé, L. Mahadevan, and P. Umbanhowar for helpful discussions. This work was supported in part by the DICyT of the University of Santiago of Chile, by the Center for Non Linear Physics and Complex Phenomena of Santiago, and by the *Catedra Presidential*.

[1] A. Lobkovsky, S. Gentges, Hao Li, D. Morse, and T. A. Witten, Science **270**, 1482 (1995).
[2] P. Stutenkemper and R. Brasche (unpublished).
[3] M. Mutz, D. Bensimon, and M. J. Brienne, Phys. Rev. Lett. **67**, 923 (1991).
[4] D. R. Nelson and L. Peliti, J. Phys. (Paris) **48**, 1085 (1987); M. Paczuski, M. Kardar, and D. R. Nelson, Phys. Rev. Lett. **60**, 2638 (1988); D. Morse, T. Lubensky, and G. Grest, Phys. Rev. A **45**, R2151 (1992); D. Bensimon, D. Mukamel, and L. Peliti, Europhys. Lett. **18**, 269 (1992); R. Attal, S. Chaïeb, and D. Bensimon, Phys. Rev. E **48**, 2232 (1993).
[5] M. Ben Amar and Y. Pomeau, Proc. R. Soc. London, Ser. A **453**, 729 (1997).
[6] The Gaussian curvature is defined as the product of the two principle curvatures, and the mean curvature is defined as the half sum of the two principle curvatures.
[7] Y. Pomeau, C. R. Acad. Sci. I, Math. **320**, 975 (1995).
[8] L. H. Donnell, Trans. Am. Soc. Mech. Eng. **56**, 795 (1934).
[9] L. Mahadevan (private communication).
[10] Th. von Kármán and H.-S. Tsien, J. Aeronaut. Sci, **8**, 303 (1941).
[11] A. Lobkovsky, Phys. Rev. E **53**, 3750 (1996).
[12] T. A. Witten and H. Li, Europhys. Lett. **23**, 51 (1993).
[13] P. Patricio da Silva and W. Krauth, Int. J. Mod. Phys. C **8**, 427 (1997).
[14] Th. von Kármán, in *Encyklopädie der Mathematischen Wissenschafen* (Forchungsarbeiten, Berlin, 1910), Vol. IV.4, p. 349.

[15] B. O. Almorth, A. M. C. Holmes, and D. O. Brush (unpublished).
[16] N. Yamaki, K. Otomo, and K. Matsuda, Exp. Mech. **15**, 23 (1975).
[17] P. Shewmon, *Transformations in Metals* (McGraw-Hill, New York, 1980).
[18] The range of the strain relief temperature is between 165 °C and 200 °C for ETP copper and between 200 °C and 250 °C for DHP copper.
[19] S. Timoshenko, *Theory of Elastic Stability* (McGraw-Hill, New York, 1951).
[20] The deflection due to vertical displacement of the border is given by the expression $w=(R^2q/Eh)(1-\nu^2)e^{-\mu x}\cos\mu x$, where ν is the Poisson coefficient, h is the thickness of the plate, q is the bending moment, and $\mu=\sqrt[4]{3(1-\nu^2)/R^2h^2}$; the length of these waves is $\lambda=2\pi/\mu\sim\sqrt{Rh}$, which is negligible with respect to the crease length and the panel length.
[21] When the crease appears, the region around the crease then acquires a zero curvature and the strip buckles like a planar plate.
[22] L. Landau and E. Lifchitz, *Théorie de l'Élasticité* (Mir, Moscow, 1967).
[23] W. T. Koiter, in *Proceedings on the Theory of Shells to Honor L. H. Donnell*, edited by D. Muster (Houston Press, Houston, 1966).
[24] H. S. Seung and D. R. Nelson, Phys. Rev. A **38**, 1005 (1988).
[25] Z. Zhang, H. T. Davis, R. S. Maier, and D. M. Kroll, Phys. Rev. B **52**, 5404 (1995).
[26] We performed the scaling by including logarithmic contributions in the bending energy; the scaling is qualitatively the same.